Eur. Phys. J. Plus (2025) 140:484
https://doi.org/10.1140/epjp/s13360-025-06370-5

THE EUROPEAN PHYSICAL JOURNAL PLUS

Regular Article

A completely non-invasive characterisation and imaging of ancient Roman "glass-gems" from Aquileia using on-site instrumentations integrated with ion beam

Giulia Marcucci[1,a], Elisabetta Gagetti[2], Maria Pia Riccardi[3,4], Quentin Lemasson[5,11], Claudia Caliri[6], Gianluca Santagati[6], Francesco Paolo Romano[6], Francesca Rosi[7], Francesca Sabatini[7,8], David Buti[9], Maya Musa[3], Marta Novello[10], Annalisa De Franzoni[10], Daniela Di Martino[1]

[1] Dipartimento di Fisica "G. Occhialini", Università degli Studi di Milano-Bicocca and INFN Sezione di Milano-Bicocca, 20126 Milan, Italy
[2] Università degli Studi di Milano "La Statale", 20122 Milan, Italy
[3] Dipartimento di Scienze della Terra e dell'ambiente (DSTA), Università degli Studi di Pavia, via Ferrata 9, 27100 Pavia, Italy
[4] Arvedi Laboratorio – sede di Pavia, Università degli Studi di Pavia, via Ferrata 9, 27100 Pavia, Italy
[5] UAR3506 Lab-BC, Ministère de la Culture/CNRS/Chimie ParisTech, 14 quai François Mitterrand, 75001 Paris, France
[6] CNR-ISPC, Via Biblioteca 4, 95124 Catania, Italy
[7] CNR-SCITEC, via Elce di Sotto 8, 06123 Perugia, Italy
[8] Department of Earth and Environmental Sciences, University of Milan-Bicocca, Piazza della Scienza 1, 20126 Milan, Italy
[9] CNR-ISPC via Madonna del Piano 10, 50019 Florence, Italy
[10] Ministero della Cultura Museo Storico e il Parco del Castello di Miramare – Direzione regionale musei nazionali Friuli Venezia Giulia -Museo Archeologico Nazionale di Aquileia, via Roma 1, 33081 Aquileia (Udine), Italy
[11] C2RMF, 14 quai François Mitterrand, 75001, Paris, France

Received: 26 September 2024 / Accepted: 27 April 2025

Abstract Since Antiquity, glass has also been used to imitate natural gemstones, leading to the development of new recipes for producing opaque and coloured glass-gems. Ancient Roman glassmakers mastered glass production, controlling both the colour and transparency. Opacity could be obtained by specific firing technology inducing microcrystalline phase formations, whereas the colour hues were influenced by specific elements with chromophore properties during glass production, such as transition metals. Proof of this expertise is the widespread of glassmaking workshops across the Roman Empire and related findings of archaeological glass artefacts still well preserved in numerous museums. The National Archaeological Museum of Aquileia (Italy) houses a rich collection of more than 6000 gems, including 1300 glass-based 'glass-gems', and not yet fully investigated. Iconographic and glyptic studies date the glass-gems from the II century BCE to the III century CE. Archaeological information on the production period, manufacturing processes and provenance can be explored by investigating the overall composition of a glass specimen. A completely non-invasive study has been carried out on a selection of glass-gems through the combination of X-ray fluorescence imaging and particle-induced X-ray/gamma emission to disclose the elemental composition, the relative distribution and gather new hints on their connection with the appearance, colour and glassmaking technology. Micro-Raman spectroscopy has been applied on opaque glass-gems to investigate the crystalline phases acting as opacifiers. Combining different non-invasive methods enables a comprehensive identification and characterisation of such glass-gems, crossing their elemental composition in terms of crystalline and glassy phases and associated key elements.

1 Introduction

The use of glass in jewellery has ancient origins (archaeological evidence can be found in Mesopotamia since the mid-third millennium BCE [1]). The advanced skills of ancient glassmakers in tuning the hues, opacity, shape, and overall appearance of glass extend their production to resemble natural gemstones with 'attractive' artificial gems. The resulting glass-gem would imitate chalcedonies, emeralds, jaspers, etc., in most cases with great success [2]. During the Roman Empire, the use of glass in jewellery was particularly widespread, favoured by the deep knowledge of Romans in glassmaking techniques and by the remarkable adaptability of this kind of material, which was much easier to carve.

One of the most influential cities in the Roman Empire regarding glass workshops was the ancient city of Aquileia, in northeastern Italy [3–7]. Its strategic location in the Roman Empire made it a hub for glyptic production and trade in antiquity. The glyptic production at Aquileia can be dated from the II century BCE to, at least the III century CE. The primary outputs of the local

[a] e-mail: giulia.marcucci@unimib.it (corresponding author)

Published online: 04 June 2025

glyptic workshops were carved natural gemstones [2, 8, 9]. Currently, Aquileia holds an exceptional legacy from Roman history and archaeological heritage, and it is one of the most important ancient Roman archaeological sites worldwide. Twenty-five years ago, the archaeological area of Aquileia, still partially unexcavated, was classified in the UNESCO World Heritage List [10].

The National Archaeological Museum (MAN) in Aquileia reflects the historical and archaeological inheritance of the ancient city with invaluable cultural heritage objects, among which one of the most important and rich collections of more than 6000 gems [8, 11]. Studying such a huge number of these artefacts is an exceptional occasion, also from a statistical point of view, which can provide precious insights into the provenance, manufacturing techniques of specific historical periods and/or geographical locations and trades in Antiquity. In this perspective, a completely non-invasive campaign has been aimed to characterise thoroughly a large selection of hundreds of glass-gems kept in MAN in Aquileia [8]. This project, named 'GEMMAE' (Glass-gems Exploration by Multidisciplinary Methods, Analyses and Experiments) [12–14], proposes new protocols based on the sole use of non-invasive methods to study the composition of glass-gems in several aspects (elements, phases, glyptic details, …). Obtaining this wide range of information non-invasively often requires a multi-technique approach, as demonstrated by previous characterisations of glass-based samples, such as historical mosaic glasses [15, 16]. In this way, different advantages can be exploited, such as the non-invasiveness and relatively short measurement times of both X-ray fluorescence (XRF) and Raman spectroscopy, the sensitiveness of Raman spectroscopy to both amorphous and crystalline phases, the XRF spatial information for a wide range of elements and the quantitative information of particle-induced X-ray/gamma emission (PIXE/PIGE). This study describes the effectiveness of combining spot elemental and phase measurements with imaging analyses extended to the entire object to study morphologically and, for some of the methods, in situ, a set of samples from a vast museum collection. This approach allows for mapping the distribution of elements and identifying any distinctive features of the gems, integrating spatial information with chemical and quantitative details.

2 Research aim

This work focuses on recent results obtained through in situ XRF mapping combined with micro-Raman spectroscopy accessing the portable instrumentation of the MOLAB (MObile LABoratory) platform of the European Research Infrastructure for Heritage Science (E-RIHS, www.e-rihs.it), integrated with previous elemental PIXE/PIGE analyses [12, 13]. We will present results for a subset of samples selected from the vast MAN collection, concerning three specific glass-gems classes described in Sect. 3.1.

The project aims to propose a non-invasive protocol by coupling the advantages of the different techniques employed to obtain in situ the elemental and crystalline phases characterisation, deducing their relation with colour and opacity of a high number of the glass-gems. The protocol relies on employing in situ instrumentations to analyse a large number of samples in a few days (a typical time duration of this kind of campaign). This step allows mapping the elemental distribution within the various morphological features of the selected glass-gems, despite their different nature (glass-based or metallic details). Potentially, the addition of a mobile Raman spectrometer provides more specific insights into the role of certain elements (e.g., through the identification of opacifiers). The chemical details accessible through this kind of campaign are useful to guide the selection of a restricted number of samples for more in-depth investigations with other non-invasive analytical techniques (or the employment of large-scale facilities) able to address any unresolved doubts.

This approach can be particularly appreciated by museums having exhibition or conservation needs affecting the possibility of moving outside a large number of objects. Moreover, PIXE/PIGE quantification crosses the elemental compositions in a complementary way, accessing the detection of a wider range of elements and therefore confirming more precisely the inferred information about the nature and production of the artefacts.

3 Materials and methods

3.1 Glass-gems samples

A subset of 19 glass-gems belonging to the Museum collection have been catalogued into three different classes and characterised: the inlaid glass-gems, the Nicologlasgemmen, and the Eros and Psyche glass-gems. A description and pictures of these artefacts are illustrated in Table 1.

Within the museum collection, the inlaid glass-gems are characterised by a bluish matrix with inlays representing different figures (e.g., animals or leaves), some of which are made of a different colour from the matrix and are likely due to metal impressions or with a golden wire. Some of these gems have a back opaque white layer [2, 8, 9].

Similar two-layer structured glass-gems are the Nicologlasgemmen, a German technical term describing glass-gems which mimic the layering and colours (pale blue on dark brown) of natural nicolo—a naturally banded variety of chalcedony, usually engraved on the lighter front surface to display figures in the darker layer. Nicologlasgemmen were produced from the late I century BCE to the early III century CE and they appear spread all over the Roman empire. The front layer is always the light blue one, which in most cases appears thoroughly engraved so that the iconography (or parts of it) appears 'en silhouette' in the colour of the back layer.

Table 1 Analysed glass-gems with archaeological information. These data, processed as part of the project to reorganise and catalogue the museum's glyptic collection launched in 2017 with the collaboration of E. Gagetti, are extrapolated from the database of the National Archaeological Museum of Aquileia, which can be partially consulted online and is constantly being updated [17]. The dimensions of the specimens are given in terms of length (L), width (W) and depth (D)

Sample code	Sample picture	Class	Dimensions L x W x D (cm^3)	Description	Dating
I.49		Inlay	$1.4 \times 1.0 \times 0.3$	Translucent cobalt blue on opaque white glass, with opaque pale green inlay representing a grapevine leaf with a stem	I century CE
I.50		Inlay	$1.3 \times 1.0 \times 0.3$	Translucent cobalt blue glass with an opaque pale green inlay representing a grapevine leaf with a stem	I century CE
I.51		Inlay	$1.0 \times 1.6 \times 0.2$	Translucent cobalt blue on opaque white, with an inlay representing a parrot	I century CE
I.52		Inlay	$1.0 \times 1.4 \times 0.2$	Translucent cobalt blue on opaque white, with an inlay representing an acanthus tuft	I century CE
I.53		Inlay	$1.2 \times .0.8 \times 0.2$	Translucent cobalt blue on opaque white, with opaque pale yellowish inlay representing a lizard	I century CE
I.54		Inlay	$1.2 \times 0.9 \times 0.2$	Translucent cobalt blue over opaque white, with an inlay representing a butterfly in flight, wings raised, in profile facing right. The iconography is outlined by a very thin gold ribbon, partly raised from its housing [17]	I century CE
I.55		Inlay	$1.2 \times 1.0 \times 0.2$	Translucent cobalt blue glass with an opaque pale yellowish inlay representing a grapevine leaf with a stem	I century CE
I.56		Inlay	$0.9 \times 1.2 \times 0.3$	Translucent cobalt blue on opaque white, with an eagle with open wings. The material once filling this shape is completely lost. The outline of the inlay presents a more intense golden colour. Probably a golden wire was used, however, it is not preserved	I century CE

Table 1 continued

Sample code	Sample picture	Class	Dimensions L x W x D (cm^3)	Description	Dating
I.57		Inlay	$1.7 \times 1.8 \times 0.2$	Translucent cobalt blue with opaque pale yellowish inlay representing a grapevine leaf with a stem A fragment of gold ribbon is preserved on the stem	I century CE
N.93		Nicologlasgemme	$1.2 \times 0.9 \times 0.2$	Opaque light blue over a translucent dark blue glass. The front surface has an iconography engraved representing the bust of a philosopher	Late I century BCE—I century CE
N.94		Nicologlasgemme	$1.2 \times 0.9 \times 0.3$	Opaque light blue on a translucent dark blue glass. The front surface has an iconography engraved representing an alighting Victoria, in profile to the left, holding a wreath and a palm branch	Late I century BCE – I century CE
N.95		Nicologlasgemme	$1.2 \times 0.9 \times 0.3$	Opaque light blue over a translucent dark blue glass. The front surface has an iconography engraved representing an alighting Victoria, in profile to the left, holding a wreath and a palm branch	Late I century BCE – I century CE
EP.35		Eros and Psyche	$1.8 \times 1.4 \times 0.5$	Monochrome opaque white glass-gem. Two winged childish figures embracing each other. On the left, a nude male figure, standing, resting his weight on the left leg, with the bust three-quarters to the right and the head in profile. The right arm is on the shoulder of the female figure, with butterfly wings, hair gathered in a bun at the top of her head and wearing a chiton. She keeps her left arm around the waist of her companion [17]	Probably I century CE
EP.37		Eros and Psyche	$1.9 \times 1.4 \times 0.6$	Monochrome transparent light greenish-blue glass-gem. The same figures of Eros and Psyche described for the gem EP.35 are engraved	Probably I century CE

Table 1 continued

Sample code	Sample picture	Class	Dimensions L x W x D (cm^3)	Description	Dating
EP.39		Eros and Psyche	$1.7 \times 1.3 \times 0.5$	Colourless transparent glass-gem. The same figures of Eros and Psyche described for the gem EP.35 are engraved	Probably I century CE
EP.40		Eros and Psyche	$2.0 \times 1.4 \times 0.6$	Monochrome opaque white glass-gem. The same figures of Eros and Psyche described for the gem EP.35 are engraved	Probably I century CE

Nicologlasgemmen were largely used as seals, set in the bezels of finger-rings. Size, shape, and section of these glass-gems vary largely (truncated cones with an elliptical base and tablets are the most common shapes), according to the changes in finger-rings fashion over time [2, 8, 9, 18]. The collection of the National Archaeological Museum of Aquileia conserves 246 glass-gems of the Nicologlasgemmen class. Four of them, displayed in Table 1, have been considered in this work.

Nicologlasgemmen N.94 and N.95 are very similar to each other not only stylistically, but also in many details. The other glass-gem of the Nicologlasgemmen class, N.93, has different shape, a lighter colour and different iconography engraved in the glass (identified as a reproduction of a bust of a philosopher).

The Eros and Psyche (below EP) class comprises a large series of monochrome glass cameos, 13 of which are stored in the National Archaeological Museum of Aquileia. These glass-gems were also widely spread in the Roman world and produced within a limited range of time, probably in the I century CE. The group is extremely homogeneous in terms of size (average sizes: $1.9 \times 1.4 \times 0.6$ cm^3), shape (elliptical), cutting style (crown: cabochon; pavilion: flat), and iconography (Eros and his lover Psyche, both winged, in each other's arms). Only some minor variants can be detected within this class, the production of which must have been clustered also in space. These glass-gems can be completely transparent, semi-transparent, translucent or opaque. Their colours are mainly hues of green, blue, and white; some can also be colourless. Their function was not aimed at jewellery but, rather, at decorating small implements of furniture, probably caskets. Though, until today no glass-gem of this class has been found in connection with its original support [2, 8, 9]. Within the aim of this manuscript, two opaque and two transparent EP glass-gems, as shown in Table 1, have been discussed.

3.2 XRF imaging

A mobile XRF scanning system developed at the XRAYLab laboratory of CNR-ISPC (Catania, Italy) has been moved in situ and employed for performing real-time elemental imaging with high spatial resolution [19, 20]. This instrumentation allows the detection of elements starting from Si up to heavier elements, such as Pb. The system consists of a spectrometric measuring head equipped with a microfocus X-ray tube with a 30 W Mo anode coupled with a focusing polycapillary lens (minimum beam size of 27 μm at the energy of the Mo Ka-line and at 9.7 mm of focus distance). X-ray fluorescence signal induced by primary radiation is revealed in event mode by a 50 mm^2 SDD with energy resolution < 130 eV at 5.9 keV. The X-ray source and detector are arranged in a 45°-45° geometry relative to the sample surface. The spectrometric head includes a long-distance optical microscope with a focal range of about 20 cm and a very short depth of field of 19 μm. The microscope is positioned along the normal direction to the sample surface and its reduced depth of field enables the accurate positioning of the sample surface at the focus distance of the primary X-ray beam, pre-aligned with the microscope's focus.

The sample is mounted on a 3-axis system (XYZ) with a stroke of $20 \times 20 \times 20$ cm^3 and the scanning is operated in continuous mode with a maximum scanning speed of up to 50 mm/sec. The system is fully managed and controlled by a custom-developed control unit (CU) for the real-time control of all sensors and all measurement operating parameters in the scanner. Further, the CU manages the real-time processing of experimental data, and the elemental images are created during scanning by applying on pixel spectra the least square fitting procedure. The elemental images are ready to be interpreted and discussed at the end of the measurement. Gems were scanned with a lateral resolution ranging between 150 and 300 μm to accommodate their size and small details. XRF imaging was operated in continuous mode by setting a dwell time per pixel of 0.2 s. The primary source was set at 50 kV and 0.6 mA during the scanning.

3.3 Particle-induced X-ray/Gamma Emission

Ion beam PIXE analyses were performed at the newAGLAE facility (Centre de Recherche et Restauration des Musées de France-C2RMF, France).

A 3 MeV proton beam 50 μm wide is driven to the samples for the analysis and five SSD-EDX detectors are used for the PIXE mode: one dedicated to the detection of low energy X-rays (1–10 keV) using a helium atmosphere; the other four detectors dedicated to the detection of high-energy X-rays (3–40 keV) for trace elements [21]. Elements with $Z > 11$ can be identified and quantified with a lower detection limit for high atomic numbers, complementarily integrating the composition of the samples investigated through XRF mapping, particularly in terms of Na, Mg and Al. Regarding sodium, its concentration is usually measured in parallel with an ultrapure germanium detector which detects γ-rays from 60 keV to 2 MeV for PIGE analysis [22].

To reduce inhomogeneity effects on the micrometre scale, the composition is evaluated over each $500 \times 500\ \mu m^2$ wide scans, with 25 μm of pixel resolution, reaching a sub-millimetre area.

However, it is worth mentioning other problems possibly affecting the measurements, like non-planar surface or the presence of inclusions, which cannot be easily overcome due to the nature of the investigated artefacts [15].

Data analysis was performed following the procedures described in [21]. Precise quantitative measurements of sample composition were calibrated regularly by using a set of calibration references, in particular standard glasses like Corning A, B, and D [23, 24] and resulting compositions are given in terms of oxides. Errors can be estimated as in [25], with values ranging from 1 to 10%, depending on the concentrations.

3.4 Raman spectroscopy

Micro-Raman spectroscopy has been applied to distinguish artefacts made of natural gems or glass-gems and, in the case of these latter, to identify mineralogical phases used as opacifiers dispersed in the vitreous matrix.

Two portable BWTEC i-Raman Plus spectrometers have been used, equipped with a 532 nm and a 785-nm laser source and two specific CCD detectors for each laser.

As expected, the system equipped with the higher energetic laser line (532 nm) gave better results being particularly suitable for studying the almost inorganic-based objects investigated. The dimension of the investigated glass-gems enabled the use of a micro-probe camera equipped with different objectives to tune the lateral resolution (4 × , 20 × , 40 × and 80 × , which correspond to investigation areas of 300–400, 90–100, 40–50 and 15–20 μm in diameter, respectively). The light emitted by the 532 nm laser was focused through an optical fibre (diameter of 105 μm) into the optical microscope. The backscattered Raman light was collected by a second optical fibre (diameter of 200 μm) and led to a 2048-element High Quantum Efficiency Back-Thinned CCD Array detector kept at -2° C by a thermoelectric cooler.

The available spectral window of the portable 532 nm Raman spectrometer is 65–4200 cm^{-1} with a spectral resolution better than 4–5 cm^{-1}. Measurements were performed with a laser power of 40 mW, using the 80 × long working distance objective investigating an area of about 15–20 μm in diameter. The exposure time of each measurement was 30 s, with 20 accumulations.

4 Results and discussion

Before discussing in detail the results obtained from the application of this non-invasive protocol, considerations on the advantages and limitations of each technique employed are given below, with the view to aiding in the design of a comprehensive analytical strategy for historical glass-based artefacts.

The analysis of materials, particularly in the context of glass, requires a combination of complementary techniques, especially when a non-invasive approach is followed. Each method belonging to this class has its strengths and limitations, making it necessary to use a multi-technique approach to obtain a comprehensive understanding of the sample composition. XRF imaging is particularly useful for determining the elemental composition of different features within a sample, and it is very well suited for mobile setups. The mapping of several batches of samples is quite fast, allowing the extension of the investigation to large numbers. The identification of variations in the composition of glass matrices, particularly in relation to colour, can be done by exploiting the wide range of elements that can be detected. Non-glass details (e.g. metallic inserts) do not limit the capacity of this technique. However, it has some limitations. While it can partially answer questions about the composition and distribution of elements, it does not provide conclusive information about the functional role of specific elements in the glass structure. Additionally, it lacks sensitivity to lighter elements and does not offer quantitative data, making it necessary to complement this analysis with other techniques.

Raman spectroscopy is highly valuable for directly identifying opacifiers in opaque glass. This technique is particularly effective in distinguishing different compounds responsible for opacity. However, it has some significant drawbacks. The presence of fluorescence can interfere with the Raman signal, reducing its effectiveness in certain samples. Additionally, as a point-based technique, it provides localised information rather than an overall picture of the bulk composition. This makes it less effective for large-scale mapping or for analysing compositional variations across an entire object.

Table 2 Glass-gems wt% composition determined by PIXE/PIGE. The table displays the major components describing the glass matrix and key elements associated with the final appearance or different features of the samples. For the inlaid and Nicologlassgemmen samples, average values evaluated over all the samples are provided as a general description of the class composition. The table includes the measured concentration for the Corning standard glasses (A, B and D)

Family and description	Na_2O	MgO	Al_2O_3	SiO_2	P_2O_5	SO_3	Cl	K_2O
Inlaid, average blue matrix	17.9	0.61	2.6	64.6	0.15	0.40	0.88	0.86
inlaid, average white matrix	15.5	0.77	3.3	58.5	0.27	0.62	0.64	0.83
inlaid, green leaf	9.1	1.6	4.9	46.4	0.88	0.83	1.3	1.9
Nicologlasgemmen front surface	14.5	0.86	3.5	59.6	0.33	0.84	0.64	1.1
Nicologlasgemmen, back surface	15.6	0.65	3.2	62.8	0.19	0.26	0.81	1.0
Eros & Psyche, transparent, light greenish-blue	16.1	0.6	2.8	68.9	0.21	0.19	1.2	0.59
Eros & Psyche, transparent, colourless	16.2	0.5	2.3	70.7	0.14	0.37	1.1	0.95
Eros & Psyche, opaque white	17.7	2.3	3.3	60.1	0.26	0.36	0.88	0.69
Corning A	14.3	2.3	1.0	66.9	0.10	0.18	0.11	2.8
Corning B	16.9	0.87	4.1	61.7	0.78	0.61	0.19	1.0
Corning D	1.4	3.6	5.2	56.0	3.8	0.26	0.17	11.2

Family and description	CaO	TiO_2	MnO	Fe_2O_3	CoO	CuO	Sb_2O_5	PbO
Inlaid, average blue matrix	8.7	0.06	0.92	1.7	0.17	0.28	0.01	0.02
inlaid, average white matrix	8.4	0.10	0.53	0.58	0.001	0.02	6.1	0.06
inlaid, green leaf	9.0	0.25	0.29	2.5	0.006	1.8	0.88	17.9
Nicologlasgemmen front surface	8.9	0.14	0.70	1.3	0.20	0.22	5.6	1.5
Nicologlasgemmen, back surface	7.8	0.10	1.7	3.1	0.02	0.05	0.11	0.14
Eros & Psyche, transparent, light greenish-blue	8.0	0.06	0.80	0.41	0.002	0.004	0.006	0.006
Eros & Psyche, transparent, colourless	5.3	0.13	0.39	0.62	0.002	0.003	1.0	0.20
Eros & Psyche, opaque white	6.9	0.11	0.02	0.57	0.001	0.02	4.5	2.0
Corning A	5.0	0.82	1.1	1.2	0.19	1.31	1.8	0.07
Corning B	8.5	0.13	0.26	0.36	0.05	2.9	0.51	0.47
Corning D	14.4	0.40	0.57	0.54	0.02	0.40	1.0	0.23

PIXE/PIGE is powerful techniques for mapping and quantifying a broad range of elements, particularly lighter ones that are not well detected by XRF. These methods complement XRF by providing a more complete elemental characterisation. However, their application to large sets of similar samples presents practical challenges. The need for specialised equipment (often in large-scale facilities), time-consuming analyses, and the requirement for specific authorisations for moving large sets of precious objects make large-scale studies using PIXE/PIGE demanding to implement efficiently, as in our case.

The following sections will detail the results obtained for each class of glass-gems, focusing on the composition of their different features (inlays, engravings, and layers) and, when possible, on the role played by certain elements or crystalline phases within the limits of each technique.

4.1 Inlaid glass-gems

4.1.1 Glass matrix

PIXE/PIGE measurements have been acquired on the blue layers of the inlaid glass-gems to obtain the composition in terms of major components of the vitreous paste (from sodium to iron oxides). Considering the size of the PIXE/PIGE analysis spots and the spatial scale of the XRF mapping (Sects. 3.2 and 3.3), an average composition of the blue glass estimated over the specimens is given to facilitate the comparison between the two techniques (Table 2). Based on their chemical composition (shown in Table 2), the analysed inlaid glass-gems can be classified as silica-soda-lime glasses; the potassium and magnesium oxides content below 1.5 wt% reflects the characteristic "Roman" composition and technology based on the use of natron as the source of soda, rather than plant ash [26, 27].

From the PIXE/PIGE analysis, key elements related to possible chromophore and opacifying agents acting in the inlaid gems (e.g., copper, cobalt and antimony) have also been highlighted, and the XRF maps in Figs. Figs. 1 and 2 show their distribution within the glasses and the inlays, where preserved.

4.1.2 Chromophore agents and decolourants

Among typical elements associated with chromophore ions, XRF imaging effectively reveals all the key components contributing to the final colour of the blue matrix of the gems: Cu, Co and Fe. In particular, a homogeneous distribution of iron, cobalt and copper

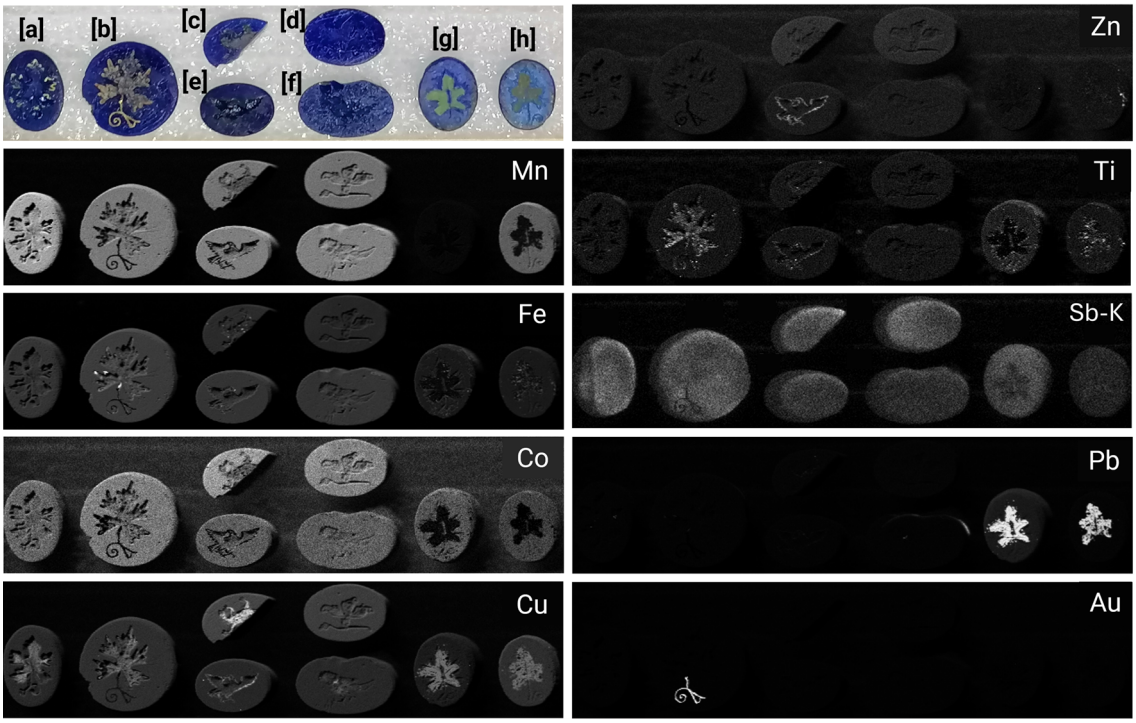

Fig. 1 XRF elemental mapping of the front blue surface of the inlay glass-gems ([a] I.49 [b] I.57 [c] I.53 [d] I.52 [e] I.56 [f] I.51 [g] I.50 [h] I.55). Lateral resolution of 150 μm and scanning speed of 1.8 mm/sec. The most relevant elements connected with the composition, colour and opacity of the glass-gems are shown

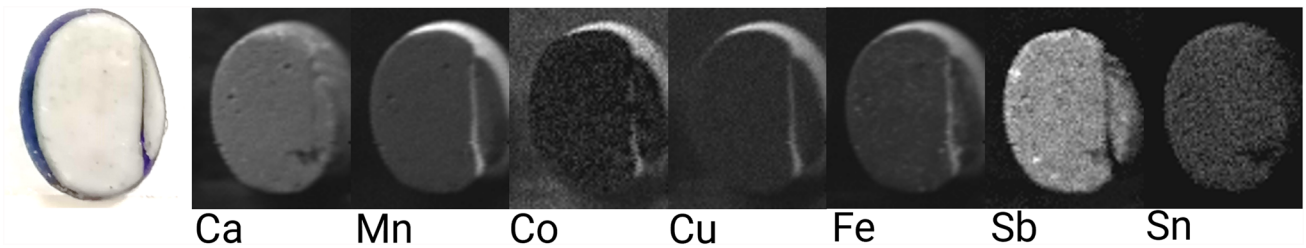

Fig. 2 XRF elemental mapping of the back white surface of the inlay glass-gem I.49. Lateral resolution of 200 μm and scanning speed of 0.4 mm/sec

can be observed in all eight front blue surfaces of the inlaid glass-gems. The mixture of these elements contributes to the intense blue colour of the glass layers hosting the inlays, as transition metal ions, such as Cu^{2+} and Co^{2+}, typically act as blue colouring agents in glass [27–30]. Moreover, the association of these elements with the blue colour is confirmed by their absence in the whitish layer, as displayed in Fig. 2. The exploitation of cobalt chromophore property was common in Roman glassmaking [19] and even rather low quantities around 100 ppm of this element are sufficient to impart the strong blue colour due to the intense absorption in the yellow region [29].

Six out of eight specimens in Fig. 1 show a homogeneous manganese distribution between the glass surface and the engraving. The exception is I.55, where the XRF signal of manganese is substantially lower only in the leaf inlay due to the Mn X-rays absorption by Pb and Cu covering the leaf.

Manganese can play a dual role in glass manufacturing, functioning as a chromophore or as a decolorising agent, depending on its oxidation state and concentration. Its presence has been well-documented in ancient glassmaking [31–33]. In certain oxidation states, particularly Mn^{3+} and Mn^{4+}, manganese imparts a distinctive colouration to glass. Mn^{3+} ions induce a purple colour, while $Mn.^{4+}$ contributes to a brownish or amber tone. The intensity and shade of these colours depend on the concentration of manganese, the glass composition, atmosphere and melting temperature conditions [31, 34, 35].

Manganese also acts as a decolouriser in glass, particularly in the removal of the greenish tint caused by iron, the main impurity in raw materials. While achieving a specific colouration is often a primary objective, the ability to produce colourless glass was equally significant in ancient times. The manufacturing of colourless glass was considerably more challenging [36]. In many cases, manganese serves as a bleaching agent, helping to neutralise the effects of iron and enabling the production of clear glass from iron-containing raw materials.

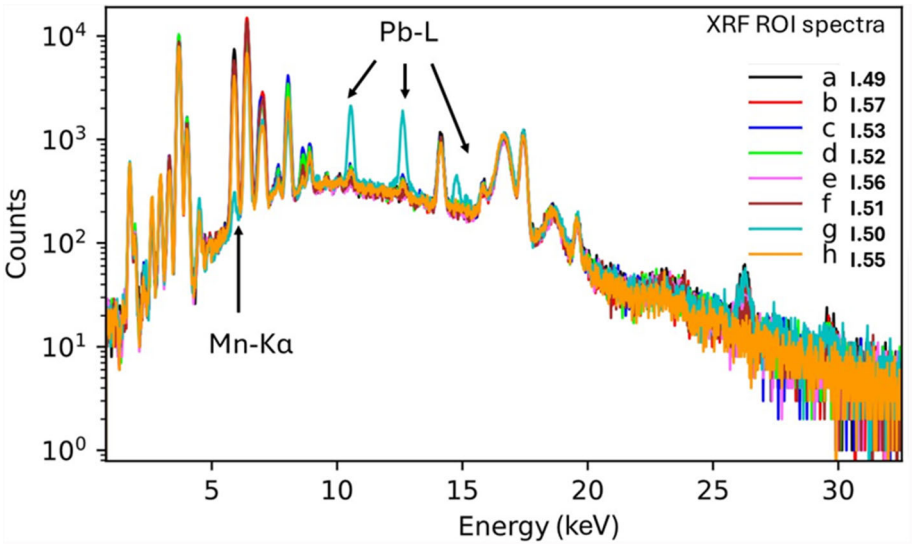

Fig. 3 XRF spectra resulting from X-ray mapping and extracted from a 10×10 pixel area selected on the glass matrix excluding the contribution of the inlay. The comparison between the spectra reveals a lower Mn content in the I.50 and, simultaneously, a higher contribution of Pb

However, this protocol does not take oxidation states into account. Their identification can resolve more precisely the role of manganese in these blue glass-gems. Additionally, the objects are stratified and contain multiple chromophores. This could make it challenging to obtain precise information from an absorption spectrum using a portable instrumentation. Therefore, the use of bench-top setups is suggested.

A completely different case is I.50, where the manganese signal is lower than the others on the whole surface. By extracting the XRF spectra on the glass matrix of all the inlaid glass-gems (excluding the inlay), a higher contribution of Pb is visible exclusively for I.50, which may be linked to the lower manganese content as shown in Fig. 3, and confirms the slightly enhanced Pb distribution visible in the XRF map.

Despite this variance, there are no discernible differences in their colouration. Hence, it is plausible that a distinct glassmaking process may have been employed in crafting I.50 compared to the other inlaid glass-gems. Due to the particularly different features of this glass-gem, a more in-depth analysis has been carried out subsequently and integrated results are given in [37].

At the level of the XRF imaging spatial resolution (hundreds of microns), the maps demonstrate the homogeneous distribution of the discussed elements within the blue matrix. The quantitative data obtained through PIXE/PIGE provide complementary information on lighter elements such as sodium, magnesium, and aluminium, which are not detectable with XRF, thus completing the description by providing the type of glass of the gems.

4.1.3 Opacifiers

Most of the glass-gems of the inlaid class present an opaque white layer placed beneath the blue surface. Figure 2 shows qualitatively the elemental composition of this substrate for the glass-gems I.49: the opacity and white colour can be attributed to the homogeneous distribution of calcium and antimony, which can be related to the presence of Ca-antimonate crystalline phases, common white opacifiers of the Roman glassmaking [38, 39]. The scatter plot in Figure S.1 supports the correlation between calcium and antimony. Quantitative PIXE measurements have revealed 8.4 wt% and 6.1 wt% as average CaO and Sb_2O_5 concentration, respectively. Other elements typically related to opacifiers (such as Sn and Pb) have been measured as traces.

The presence of antimony evidenced by XRF imaging and quantified as a major component in the white substrate of these glass-gems suggests the use of antimony-based crystalline phases to impart opacity, a very common practice in Roman times and thus consistent with the proposed dating for the inlay class.

4.1.4 Inlay composition

From the point of view of the inlaid subjects, some glass-gems have yellowish/greenish engraved iconographies (e.g., the four artefacts with grapevine leaves and the one with, probably, a lizard), while for the remaining ones, only a few traces of a possible different colour remained in the inlay. Presence of copper in varying concentrations was detected by XRF mapping in the inlaid except for the eagle (I.56) and the acanthus cluster (I.52). Samples I.50 and I.55 are stylistically very similar. The XRF elemental mapping also reveals similarity in terms of the elemental composition of the inlay (Fig. 1): in correspondence with the greenish leaf copper and lead appear to be linearly correlated (Fig. 4), suggesting that they are mixed to produce the greenish colour. Further details about the origin of the lead in the leaf are provided in [37]. Traces of titanium are visible in the leaf region of glass-gems I.57 and I.55.

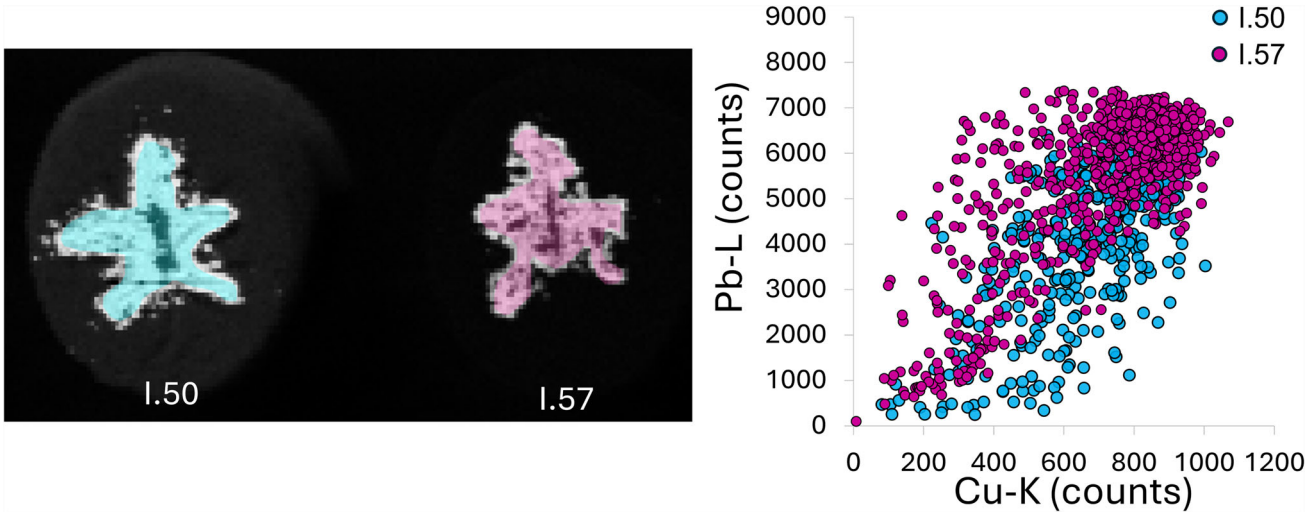

Fig. 4 Cu-K/Pb-L scatter plot by extracting the net counts from the greenish leaf decoration of the I.50 and I.55 glass-gems

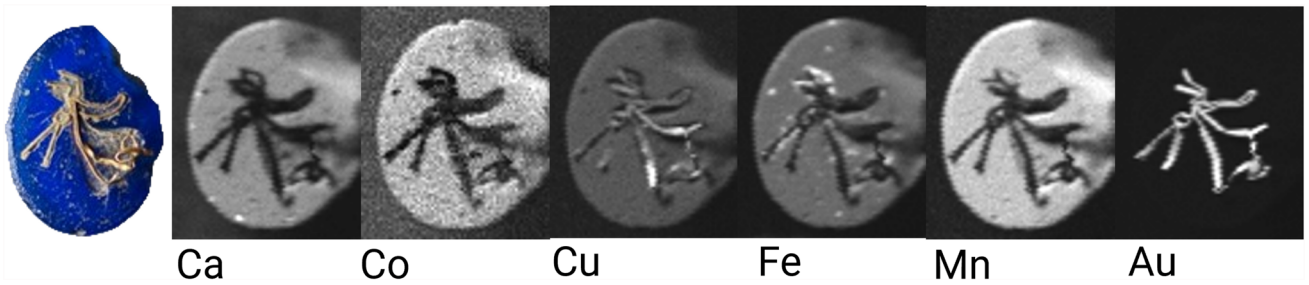

Fig. 5 XRF elemental mapping of the inlay on glass-gem I.54. Lateral resolution in both vertical and horizontal directions has been set to 150 μm

The specimen with an eagle, instead, has a copper distribution along the inlay outline and another interesting detail is the distribution of zinc in the outline, probably indicating the use of a wire made of brass for the inlay. An additional evidence of the employment of metallic wires for inlaying these gems can be found in the stem of the vine leaf of I.57 and on the entire figure representing a butterfly in I.54, both made of gold, as shown in Fig. 1 and Fig. 5, respectively. In particular, XRF imaging on I.54 also reveals the presence of silver in the entire wire (Fig. 6); an inhomogeneous distribution of copper and iron seems added below the wire, between the inlay and the glass surface. PIXE distribution maps of Cu, Ag and Au in a section of the butterfly are shown in Fig. 7, along with sodium and cobalt related to the vitreous medium hosting the inlay.

It is most likely that the inlays were surrounded by a thin gold-coloured metallic wire. However, looking between the butterfly inlay, the petiole of the vine leaf, and the eagle inlay, the nature of this wire can vary between a gold-based alloy and brass.

4.2 Nicologlasgemmen

4.2.1 Glass matrix

The chemical composition of the Nicologlassgemmen, retrieved through PIXE/PIGE measurements and detailed in Table 2, identifies them as silica-soda-lime glasses. Also in this case, their low potassium and magnesium oxide content (less than 1.5 wt%) indicates natron as the soda source, distinctive of the Roman glassmaking tradition [26, 27].

4.2.2 Chromophore agents

XRF imaging has been performed on the front engraved surface of three Nicologlasgemmen, two of which are stylistically similar (N.94 and N.95 – the pair with the alighting Victoria) while the third (N.93) has a different shape and a lighter colour in the engraved layer. The resulting elemental maps are displayed in Fig. 8: XRF imaging suggests that the main elements responsible for the lighter blue colour of all the front engraved surfaces are cobalt, copper, manganese, and iron, the latter apparently in different amounts between the Victoria pair and the Philosopher. Moreover, it can be noticed a homogeneous distribution between the front layers and the engravings for these elements. Their role in the blue colour is confirmed and integrated by PIXE analysis performed on a representative area of both the front and back layers (Sect. 3.3): the quantified CoO average content corresponds to 0.20 wt% on

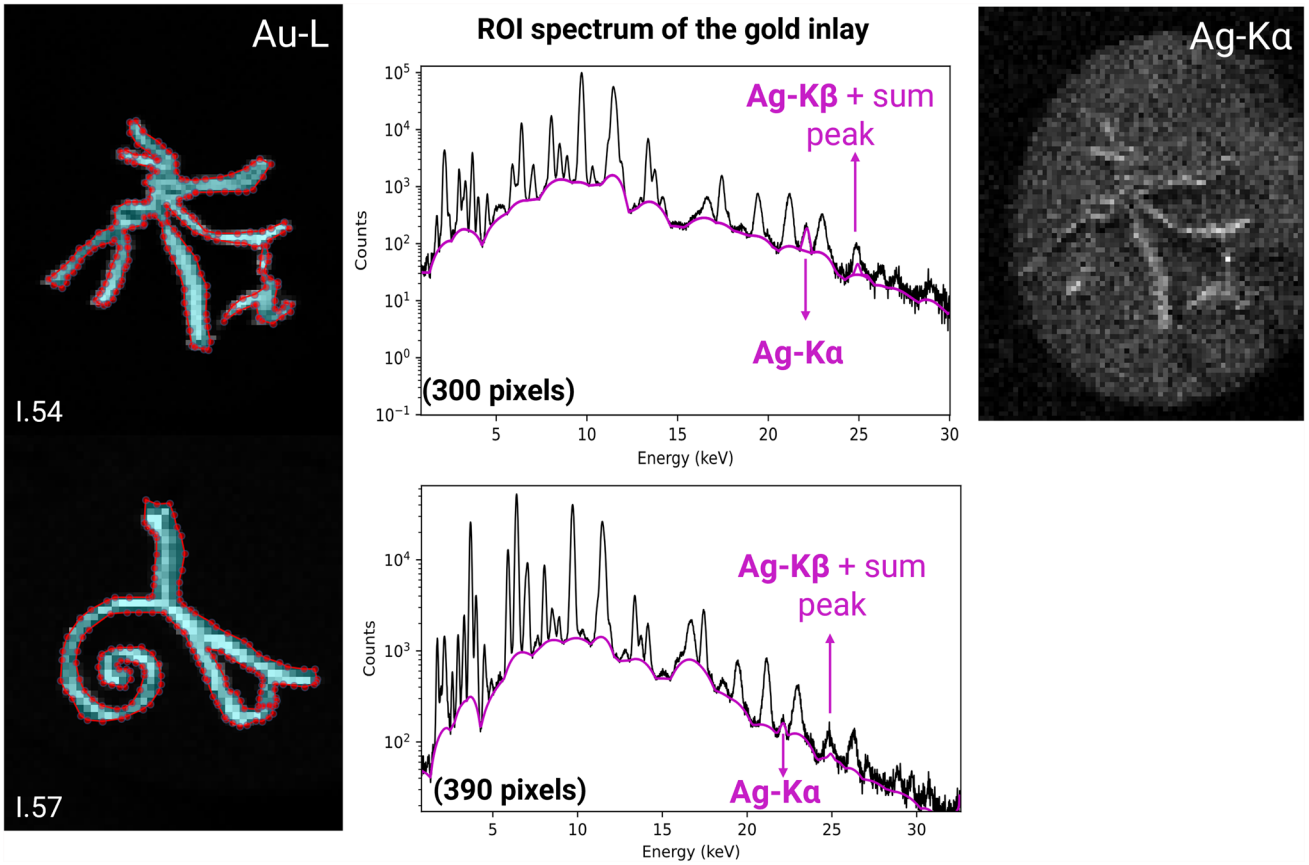

Fig. 6 Spectra extracted from the XRF dataset in the region of the gold wires of the gems I.54 and I.57 (blue outline dotted with red), where the Ag-K fluorescence signals are highlighted. The silver distribution is also displayed for I.54, while the signal-to-noise ratio of I.57 is too low to generate a significant distribution map

the front and it strongly differs from the content in the darker back layer, where it is less than 200 ppm. The iron content varies between the front (Fe_2O_3 1.3 wt%) and the back (Fe_2O_3 3.1 wt%) and the PIXE quantification of manganese, as well, revealed a higher content in the darker layer (front: MnO = 0.70 wt%; back: MnO = 1.7 wt%). Focusing specifically on the composition of the back layer, the PIXE results suggest that iron and manganese are two possible chromophore elements contributing to the final dark coloration of this layer. The overall appearance of the Philosopher's gem (N.93) macroscopically differs from the Victoria pair (N.94 and N.95), although they belong to the same typological class—the Nicologlassgemme—which is considered a homogeneous group of gems from an archaeological and iconographic perspective. In terms of visible colour, the N.93 differs from the pair of the Victoria, as well as the distribution of iron and lead highlighted by XRF imaging reflects this macroscopic colour difference. Meanwhile, the PIXE/PIGE data refer to the average of the class to investigate the composition of the glass matrix as a whole. More specific analyses in the future will focus on better understanding the nature of this difference.

4.2.3 Opacifiers

Following this tendency, the elemental mapping on the engraved blue layers also shows varying contents of Sb, Ca and Pb between the pair with the alighting Victoria and the gem with the philosopher: the former is characterised by a higher amount of lead, while the latter is more enriched with calcium and antimony. This different Ca and Sb content may be responsible for the lighter blue colour of N.93 as can be related to the presence of the white calcium-antimonate opacifiers. The scatter plot in Figure S.2 (Supplementary Material) shows the correlation between calcium and the antimony characterising the opaque light blue surface of the gem.

PIXE analysis pointed out the role of antimony in all three Nicologlasgemmen as the main element related to the presence of opacifiers. Moreover, this technique has been applied to both the front and back surfaces of the discussed Nicologlassgemmen, integrating also in this case the results obtained through XRF elemental mapping on only one side of the glass-gems. Quantitatively, the opaque blue coverings contain more antimony than the back surfaces (Table 2), which appear more translucent. Moreover, the high calcium content in the front layers makes them inherently appropriate for forming calcium-antimonate opacifiers [40].

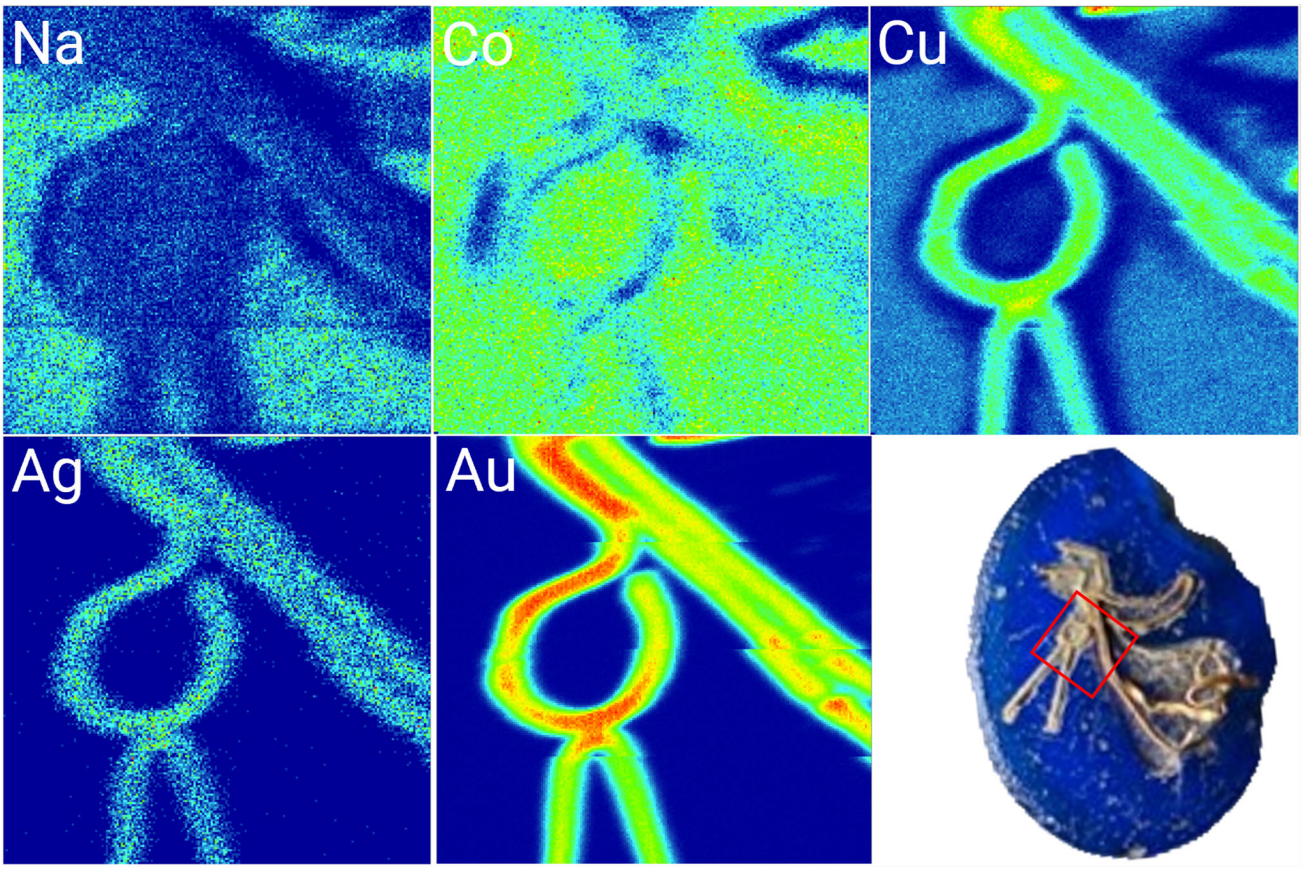

Fig. 7 PIXE elemental mapping of Na, Co, Cu, Ag and Au of a section of the inlay of I.54 (highlighted in red in the sample picture). Each map dimension is 2×2 mm^2, with 10 μs of step size

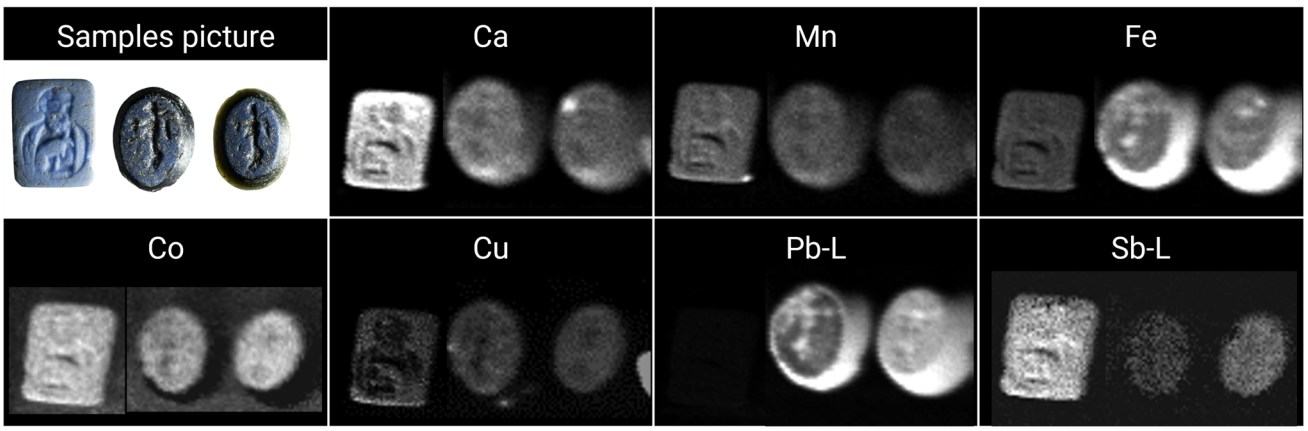

Fig. 8 XRF imaging of the distributions of most relevant elements of Nicologlasgemmen front surfaces, which are, from left to right, N.93, N.94 and N.95. Scanning parameters: 300×300 μm^2 horizontal and vertical step, 20 ms acquisition time

Calcium-antimonate opacifiers have been identified through Raman spectroscopy (Fig. 9) in the phase $CaSb_2O_6$ (main peak at 670 cm^{-1} [41]) on the opaque surface of both samples N.94 (emerging from a strong fluorescence) and N.95, while on their darker back layer, no bands ascribable to crystalline phases have been detected, as expected for a translucent glass.

The use of antimonates as opacifiers covered an extensive historical period, from Ancient Egypt to the present days, although there have been periods of interruption [42]. In particular, Ca-antimonates were the most common opacifiers of Roman glassmaking until the IV century CE [38, 39]; therefore, their detection is in agreement with the dating hypothesised for this glass-gem. Traces of tin have also been detected through PIXE/PIGE; thus, presence of tin-based opacifiers cannot be excluded. The use of them together with antimony-based opacifiers was a common practice for defined periods, such as during II-I centuries BCE. Then, from the IV

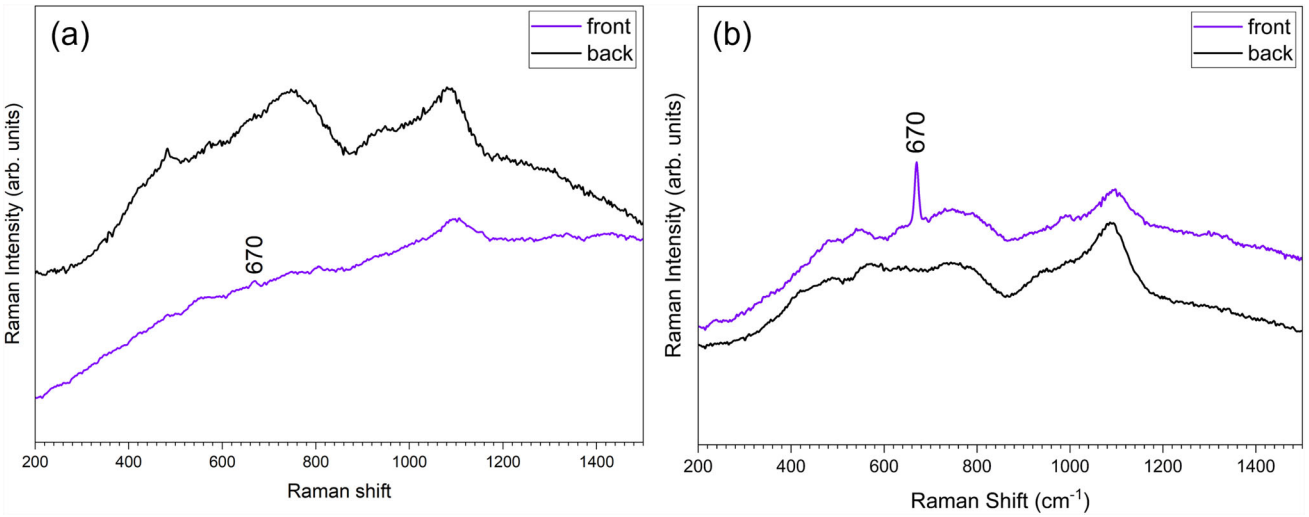

Fig. 9 Raman spectra (wavelength 532 nm) on both front and back surfaces of Nicologlasgemme N.94 (a) and N.95 (b). On the front surface of both samples, the characteristic main peak of $CaSb_2O_6$ is visible around 670 cm^{-1}

century CE, tin-based opacifiers started to replace antimony-based opacifiers in glass produced from the eastern Mediterranean through northern Europe. In Italy, from the V century CE onwards, tin-based opacifiers were also used at the same time as antimony-based opacifiers until the XIII century CE [38, 43, 44]. However, in these samples, tin is not a predominant component compared to antimony, in agreement with the expected chronological collocation.

Moreover, within the hypothesis of in situ crystallisation, the identification of the calcium-antimonate opacifiers could also be an indication of the firing temperature for all the samples: previous works on the synthesis of pure calcium-antimonate crystals [45] demonstrate that the formation of $CaSb_2O_6$ can be reached at temperatures higher than 930 °C, when this phase starts to crystallise until it becomes predominant from 1100 °C. Although the presence of only one of the two phases cannot be confirmed at this stage, due to low statistics, we can hypothesise at least a firing temperature range higher than 930 °C for samples N.94 and N.95. An upper limit can also be indicated at 1200 °C based on the literature; indeed, ancient glassmakers were not able to exceed them [45–48]. Furthermore, the Pb content in N.94 and N.95 could be correlated to a flux effect, able to reduce the melting temperature of the glass lower than 1200 °C during the process of opacification [49].

4.3 Eros and psyche glass-gems

XRF mapping has been conducted on two transparent and two opaque glass-gems belonging to the Eros and Psyche class. In addition, the elemental composition of this set of glass-gems has been investigated through PIXE/PIGE analysis (Table 2): all four samples are characterised by a natron-based glass matrix, while elemental differences directly emerge from the XRF mapping. Figure 10 displays the distribution of the most interesting elements (Ca, Mn, Fe, Co, Cu, Pb and Sb) that characterise their composition. The main differences between the transparent and opaque pairs are in terms of Mn, Sb and Pb content. In particular, the two opaque EP gems show a higher concentration of antimony than the transparent pair. Variations are also evident even though the two opaque gems: EP.40 exhibits stronger saturation for lead while EP.35 shows a higher antimony concentration. Therefore, a different recipe was used not only in the production of gems with different transparency but also between the two artefacts with similar opacity.

Moreover, the presence of antimony can be correlated to that of calcium in the opaque gems EP.40 and EP.35 (Figure S.3), an indication of antimonate opacifiers formation in the glass. Another possible source of opacity is typically tin. However, it was not detected in a relevant amount through XRF imaging.

The presence of lead is also responsible for the yellowish colour of glass-gem EP.40 and can be associated with either an addition as glass former or the presence of lead-based opacifiers [28]. The Pb-L/Sb-L correlation plot in Figure S.4 supports the latter hypothesis.

On the other hand, the two transparent EP gems are marked by an enhanced presence of Mn: this element often plays the role of a decolouriser leading to uncoloured glasses [36 and references therein]. Calcium is also highly saturated in the light greenish-blue gem. The other transparent sample contains a remarkable but less content of Ca, estimated to 5.3 wt% with the quantitative analysis. The calcium content in these glass-gems, despite the macroscopical aspect differences in terms of opacity with the other two E&P specimens, reflects the Roman basical glass recipes (mostly identified as soda-lime-silica glass), as described in [3, 5, 36], and therefore, it does not have an effect on the opacity of the glass but rather as a stabiliser.

The quantitative concentration of major and key elements characterising the opaque gem EP.40 is displayed in Table 2.

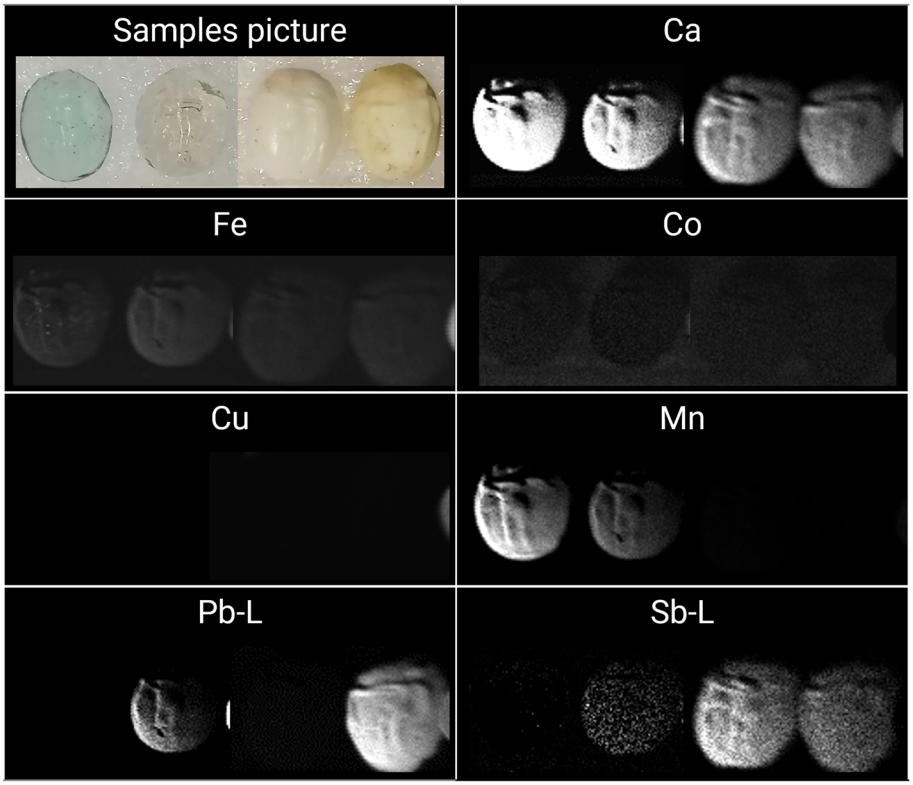

Fig. 10 From left to right in the sample picture: the two transparent gems, EP.37 and EP.39, and the two opaque gems, EP.35 and EP.40. The main elements mapped by XRF imaging and related to the colour and opacity of the samples are shown

5 Conclusions

A combined approach of in situ and large-scale facilities analyses has been proposed to investigate in a completely non-invasive way the composition of glass-gems selected from a wide collection of thousands of artefacts kept at the National Archaeological Museum of Aquileia, to disclose further insights into Roman glass composition useful for deriving information about ancient production methods and recipes. The aim of this article is not to provide an in-depth exploration of archaeological questions, including dating and provenance, which require more specific details and a thorough comparison. Rather, this work emphasises the results obtained by mobile XRF imaging, concerning the relationship between elemental distribution, colour and opacity of the investigated artefacts. The selected samples have particular features such as inlays, engravings and layers with a different appearance to the main matrix. The elemental mapping revealed the key elements responsible for the final colour and opacity of the glass-gems, along with their distribution across all their features. It also demonstrated versatility by measuring both glass and metal elements in a single measurement, such as in the case of the inlaid samples. Moreover, correlation information between two elements can be extracted with this technique, supporting hypotheses regarding the presence of certain crystalline phases, such as calcium or lead antimonates.

The integration of elemental mapping with PIXE/PIGE and Raman spectroscopy measurements exploits the strengths of each non-destructive method in a complementary way and overcomes their limits in providing a comprehensive description of the gem composition.

When comparing XRF mapping with PIXE/PIGE, it is important to note that, although they are both elemental techniques, significant differences in the results collected might be evidenced. Firstly, the spatial resolution and sensitivity to light elements is different. The PIXE/PIGE technique provides crucial information on light elements, in particular sodium, significant for understanding the composition and properties of glassy samples. Furthermore, PIXE/PIGE measurements enable the completion of the elemental description by providing the quantitative concentrations of key elements identified with the XRF mapping. Within the mobile operating condition of this study, the XRF investigation of light elements is compromised due to the need to see heavier and trace elements present in details such as the inlays. PIXE/PIGE analysis has been complementary but also preparatory for XRF imaging, which is faster in mapping the elements of interest once identified with PIXE (e.g., the investigation of lead or gold distribution). From an iconographic and archaeological point of view, the classes of inlaid glass-gems, Nicologlassgemmen, and Eros&Psyche are considered homogeneous. However, compared to the Inlay class, the Nicologlassgemmen and Eros&Psyche glass-gems are more variegated. The analyses carried out on the gems presented in this manuscript, which represent only a limited selection for each class, have shown that for Nicologlassgemmen and Eros&Psyche, the visible aspects of the material (such as visible colour and opacity) and consequently the composition of the material itself exhibit both similarities and differences. These

correspond to those observable macroscopically (e.g., the different shades of blue in the Nicologlassgemmen linked to the varying elemental distributions highlighted through XRF mapping). Regarding Eros&Psyche glass-gems, starting from the same base material as evidenced by PIXE analyses, ancient craftsmen managed to achieve different effects in terms of colour variety (ranging from transparent to opaque) by varying specific elements (e.g., manganese, lead and antimony) as revealed by XRF maps.

The complementary use of the non-destructive techniques discussed in this paper highlighted these differences, within the limitations of each technique.

More in-depth analyses will continue within the GEMMAE project, to encompass the entire volume rather than just specific points with additional complementary investigations, always with a non-invasive approach, and preferably conducted in situ at the Aquileia museum. A potential direction for future work could be the application of absorbance spectroscopy techniques to precisely identify oxidation states and chromophore groups.

Supplementary Information The online version contains supplementary material available at https://doi.org/10.1140/epjp/s13360-025-06370-5.

Acknowledgements The support by MUR (FOE ERIHS IT and PON Ricerca e Innovazione 2014-2020, CCI: 2014IT16M2OP005) is acknowledged. Financial support from the Access to Research Infrastructures activity in the Horizon 2020 Programme of the EU (IPERION CH H2020-INFRAIA-2014-2015, Grant No. 654028) is gratefully acknowledged (FIXLAB: newAGLAE, France).

Funding Open access funding provided by Università degli Studi di Milano - Bicocca within the CRUI-CARE Agreement.

Data Availability Statement This manuscript has associated data available upon reasonable request to the corresponding author.

Declarations

Conflict of interest There are no conflicts to declare.

References

1. P.R.S. Moorey, Ancient Mesopotamian Materials and Industries, The Archaeological Evidence, (Winona Lake, Eisenbrauns, 1999).
2. G. Sena Chiesa, Gemme romane in Italia settentrionale. Collezioni, studi, rinvenimenti: una ricognizione, 83 Pallas 224 (2010). https://doi.org/10.4000/pallas.11084.
3. C. Boschetti, V. Mantovani, C. Leonelli, J. Glass Stud. **58**, 69–86 (2016)
4. C. Boschetti, J. Henderson, J. Evans, C. Leonelli, J. Archaeol. Sci. Rep. **7**, 303–311 (2016)
5. J. Boschiero et al., J. Cult. Herit. **55**, 117–127 (2022)
6. M. Buora, L. Mandruzzato and M. Verità, Vecchie e nuove evidenze di officine Vetrarie romane ad Aquileia, Quaderni Friulani di Archeologia XIX/2009
7. M. Buora, Nuove osservazioni sulle attività artigianali ad Aquileia, con particolare riferimento alla lavora zione del ferro e del vetro. Quaderni Friulani di Archeologia XXV-2015
8. G. Sena Chiesa, Gemme del Museo Nazionale di Aquileia, (Padova, 1966).
9. E. Gagetti, M. Novello, Paesaggio e ambientazione nelle gemme di Aquileia. In Proceedings of the International Conference 'Iconografia 2022', (Padua-Venice, Italy, 12th-14th December 2022).
10. https://whc.unesco.org/en/list/825
11. Website of the National Archaeological Museum in Aquileia https://museoarcheologicoaquileia.beniculturali.it/ (last accessed on the 20th of December 2023).
12. D. Di Martino, et. al., J. Phys. Conf. Ser. 2022, 2204(1) (2022).
13. D. Di Martino, E. Gagetti, G. Marcucci, M.P. Riccardi, 14th International Conference on non-destructive investigations and microanalysis for the diagnostics and conservation of cultural and environmental heritage - 2023 - Brescia (Italy) (art 2023) ISBN 979–12–5544–031–4.
14. M. Musa, E. Gagetti, M.P. Riccardi, G. Marcucci, D. Di Martino, Il Nuovo Cimento, 46 C, 158 (2023).
15. G. Marcucci et al., Eur. Phys. J. Plus (2021). https://doi.org/10.1140/epjp/s13360-021-01696-2
16. G. Marcucci, A. Scherillo, R. Smith, D. Di Martino, Phys. Chem. Glas.: Eur. J. Glass Sci. Technol. B 64(2), 52–56 (2023).
17. https://www.manaquileiacollezione.beniculturali.it/login.php
18. E. Gagetti, Pallas **83**, 55–97 (2010). https://doi.org/10.4000/pallas.10690
19. H.C. Santos et al., Microchem. J. **124**, 241–246 (2016)
20. F.P. Romano et al., J. Anal. At. Spectrom. **32**(4), 773–781 (2017)
21. L. Pichon, et al., Nucl. Instrum. Methods Phys. Res. Sect. B Beam Interact. Mater. Atoms (2015). https://doi.org/10.1016/j.nimb.2015.08.086
22. I. Biron, S. Beauchoux, Meas. Sci. Technol. (2003). https://doi.org/10.1088/0957-0233/14/9/308
23. E.P. Vicenzi, S. Eggins, A. Logan, R. Wysoczanski, J. Res. Natl. Inst. Stand. Technol. **107**, 719 (2002). https://doi.org/10.6028/jres.107.058
24. B. Wagner, A. Nowak, E. Bulska, K. Hametner, D. Günther, Anal. Bioanal. Chem. **402**, 1667–1677 (2012). https://doi.org/10.1007/s00216-011-5597-8
25. M. Radepont et al., Measurement **114**, 501–507 (2018). https://doi.org/10.1016/j.measurement.2016.07.005
26. E.V. Sayre, R.W. Smith, Compositional Categories of Ancient Glass. Science **133**(3467), 1824–1826 (1961)
27. J. Bayley, I. Freestone, C.M. Jackson (eds.), *Glass of the Roman World* (Oxbow Books, Oxford, 2015)
28. D. Möncke et al., J. Archaeol. Sci. **46**, 23–36 (2014). https://doi.org/10.1016/j.jas.2014.03.007

29. I.C. Freestone, J. Glass Stud. **57**, 29–40 (2015)
30. L. Medeghini et al., Microchem. J. (2022). https://doi.org/10.1016/j.microc.2022.107526
31. D. Moncke, M. Papageorgiou, A. Winterstein-Beckmann, N. Zacharias, J. Archaeol. Sci. **46**, 23–36 (2014)
32. E. Gliozzo et al., Archaeol. Anthropol. Sci. **9**, 165–180 (2017)
33. A.I. Bidegaray et al., Archaeol. Anthropol. Sci. **12**, 1–17 (2020)
34. A.I. Bidegaray et al., J. Archaeol. Sci. Rep. **27**, 101975 (2019)
35. S. Rossano et al., J. Non-Cryst. Solids **594**, 121710 (2022)
36. E. Gliozzo, Archaeol. Anthropol. Sci. **9**, 455–483 (2017). https://doi.org/10.1007/s12520-016-0388-y
37. D. Di Martino et al., Heritage **8**, 41 (2025). https://doi.org/10.3390/heritage8020041
38. M. Tite, T. Pradell, A. Shortland, Discovery. Archaeometry **50**(1), 67–84 (2008). https://doi.org/10.1111/j.1475-4754.2007.00339.x
39. M. Verità et al., J. Glass Stud. **55**, 39–52 (2013)
40. S. Paynter, T. Kearns, H. Cool, S. Chenery, J. Archaeol. Sci. **62**, 66–81 (2015)
41. E. Basso et al., J. Raman Spectrosc. **45**, 238–245 (2014)
42. S. Lahlil et al., Appl. Phys. A (2010). https://doi.org/10.1007/s00339-010-5650-z
43. G.M. Uboldi and M. Verità, J. Glass Stud., 115–137 (2003).
44. C. Fiori, M. Vandini, and V. Mazzotti, I colori del vetro antico. Il vetro musivo bizantino. (Il prato, 2004).
45. S. Maltoni, A. Silvestri, Minerals (2018). https://doi.org/10.3390/min8060255
46. P.T. Nicholson, J. Glass Stud. **37**, 11–19 (1995)
47. K. Heide, E. Hartman, K. Gert, H.G. Wiedemann, Thermochim. Acta **365**(1–2), 147–156 (2000)
48. F. Wiesenberg, Experimentelle Archäologie: Römische Glasöfen: Rekonstruktion und Betrieb einer Glashütte nach römischem Vorbild in der Villa Borg: "Borg Furnace Project 2013". 2014.
49. C. Boschetti et al., Heritage **3**(2), 549–560 (2020). https://doi.org/10.3390/heritage3020032